Journal of Power Sources 375 (2018) 43–52

Contents lists available at ScienceDirect

Journal of Power Sources

journal homepage: www.elsevier.com/locate/jpowsour

Comparative study of imide-based Li salts as electrolyte additives for Li-ion batteries

Varvara Sharova[a,b], Arianna Moretti[a,b,*], Thomas Diemant[c], Alberto Varzi[a,b], R.Jürgen Behm[a,c], Stefano Passerini[a,b,**]

[a] Helmholtz Institute Ulm (HIU), Helmholtzstr. 11, D-89077 Ulm, Germany
[b] Karlsruhe Institute of Technology (KIT), PO Box 3640, D-76021 Karlsruhe, Germany
[c] Institute of Surface Chemistry and Catalysis, Ulm University, Albert-Einstein-Allee 47, D-89069 Ulm, Germany

HIGHLIGHTS

- Imide-based salts (LiTFSI, LiFSI, and LiFTFSI) as additives in carbonate-based electrolyte.
- Effect of imide salts on the SEI formed on graphite.
- Incorporation of imide salts in the graphite's SEI.
- Effect of imide salts on the 1st cycle coulombic efficiency in graphite/LFP cells.
- Addition of LiTFSI results in the capacity retention above 98% even after 600 cycles.

ARTICLE INFO

Keywords:
Li-ion cell
Imide salt
Additive
SEI
Coulombic efficiency

ABSTRACT

Herein, we report the results of a detailed study on the use of different Li imide salts (LiTFSI, LiFSI, and LiFTFSI) as electrolyte additives for lithium-ion batteries. The introduction of lithium imide salts in the electrolyte is shown to considerably improve the first cycle coulombic efficiency and the long-term cycling stability of graphite/$LiFePO_4$ cells. Using LiTFSI, a capacity fading of only ~2% occurred over 600 cycles while the control cell with the state-of-the-art additive (VC) lost ~20% of the initial capacity at 20 °C. The results of the XPS and impedance spectroscopy measurements of graphite electrodes show that, after the formation cycle, the SEI obtained in the presence of imide salts is thinner, contains more LiF and is less resistive than that obtained using VC. Despite the beneficial effect of the imide salts on the lithium-ion cell performance, a slightly reduced thermal stability of the SEI is observed.

1. Introduction

Lithium-ion batteries (LIBs) are nowadays largely used in portable electronics and are quickly penetrating the automotive and stationary energy storage sectors. Indeed, LIBs offer higher specific energies (150–200 Wh/kg) and energy efficiencies with respect to other rechargeable batteries, e.g., Ni-MH or lead-acid batteries [1,2].

The graphite anode used in commercial LIBs can reversibly deliver about 370 mAh g^{-1} at an operating voltage close to that of metallic lithium. One of the key factors ensuring the prolonged cycle life of the anode is the formation of the solid electrolyte interphase (SEI) as a consequence of the electrolyte reduction reaction during the first lithiation (charge of the Li-ion cell) [3]. Ideally, being electronically insulating, the SEI prevents further electrolyte decomposition, while allowing fast Li^+ ion conduction [4,5]. However, the anode's volume change during Li^+ insertion and de-insertion process causes the exposure of fresh graphite surface to the electrolyte. This generates a continuous growth of the SEI, which implies Li^+ consumption and increase of cell resistance leading to capacity fading upon cycling. Therefore, it is crucial to obtain an SEI with appropriate mechanical, chemical and thermal stabilities, electronic resistance, ionic conductivity and thickness during the formation cycle. These characteristics are determined principally by the electrolyte composition. The "state-of-the-art" electrolytes are mixtures of cyclic and linear organic

* Corresponding author. Helmholtz Institute Ulm (HIU), Helmholtzstr. 11, D-89077 Ulm, Germany; Karlsruhe Institute of Technology (KIT), PO Box 3640, D-76021 Karlsruhe, Germany.
** Corresponding author. Helmholtz Institute Ulm (HIU), Helmholtzstr. 11, D-89077 Ulm, Germany; Karlsruhe Institute of Technology (KIT), PO Box 3640, D-76021 Karlsruhe, Germany.
E-mail addresses: arianna.moretti@kit.edu (A. Moretti), stefano.passerini@kit.edu (S. Passerini).

https://doi.org/10.1016/j.jpowsour.2017.11.045
Received 2 September 2017; Received in revised form 14 October 2017; Accepted 13 November 2017

carbonates dissolving lithium hexafluorophosphate ($LiPF_6$). Although this salt suffers from poor thermal and chemical stabilities, it grants SEI formation, high ionic conductivity, relatively wide electrochemical stability window (ESW) and Al current collector passivation [6,7].

Many efforts have been devoted to link the SEI characteristics to its composition. It is generally agreed that the SEI consists of two different layers. The inner layer, in contact with the graphite surface, is dominated by insoluble inorganic components, e.g., LiF, Li_2CO_3 and Li_2O [8,9], i.e., purely ionic conductors, which prevent further electrolyte decomposition. The outer layer instead is more porous and composed of organic species, e.g., ROLi and $ROCO_2Li$ [5], which may be partly soluble in the electrolyte leading to continuous modification of the layer composition and morphology [4].

The SEI composition can be further tuned by introducing additives (usually less than 10% either in weight or in volume) in the electrolyte [6]. Reductive-type additives are decomposed at potentials higher than that of the electrolyte solvent(s) and salt(s). The widely used vinylene carbonate (VC) belongs to this category, forming a polymeric surface layer upon reduction at about 1.0 V, which enhances the cycling stability and the safety of the cell [10,11]. On the other hand, reaction-type additives are not always electrochemically reduced. Instead, they can react with electrolyte decomposition products such as radical anions, thus, stabilizing the SEI [6,12].

Lithium imide salts, e.g., lithium bis(trifluoromethanesulfonyl) imide (LiTFSI) or lithium bis(fluorosulfonyl)imide (LiFSI), have been proposed as alternatives to $LiPF_6$ due to their lower sensitivity to hydrolysis and their increased thermal and electrochemical stabilities [7,13–17]. However, being anodically more stable than $LiPF_6$, their use requires the presence of fluorinated electrolytes [18] or $LiPF_6$ as a co-salt [19] to avoid the anodic dissolution of aluminum current collector.

Dahn et al. [20] investigated the use of LiTFSI and VC as additives in different Li-ion cells by careful and precise measurement of the coulombic efficiency and end-point slippage rate. They found that the addition of LiTFSI (2–4 wt%) does not have any impact on the cycle life, but rather on the reduction of the cell impedance (especially in combination with VC), and thus, on improving the cells rate capability and capacity retention at high rates. These authors suggested LiTFSI to change the electrode surface film composition, leading to a thinner but more protective film [15]. The same group reported that the combination of LiFSI with VC can reduce the gas formation and the voltage drop at 60 °C [21]. However, presently it is not fully understood how low concentrations of Li-imide salts in the electrolyte affect the SEI composition.

Herein, we elucidate the impact of Li-imide salt addition (2 wt%) on the electrochemical performance of graphite electrodes. Three salts with different anions have been selected, namely LiTFSI, LiFSI and lithium fluorosulfonyl(trifluoromethanesulfonyl)imide (LiFTFSI), whose chemical structures are shown in Fig. S1 of the Supporting Information. The electrochemical characteristics of half and full cells, as well as the surface composition of the graphite electrodes, are compared with those of electrodes cycled using the pure and VC-added electrolytes.

2. Experimental

2.1. Electrodes and electrolytes

The calendered graphite and $LiFePO_4$ (LFP) electrodes were kindly provided by CEA-LITEN. The graphite electrodes, comprising 95% of active material and calendered to a porosity of 39%, had an average loading of 8 mg cm^{-2} (~2.75 mAh cm^{-2}). The LFP electrodes with 90% of active material and 35% porosity had an average loading of 17.5 mg cm^{-2} (~2.5 mAh cm^{-2}), determining an anode/cathode capacity ratio of 1.1 for the graphite/LFP Li-ion cells. The electrodes for the electrochemical stability window test comprised 80% of CMC binder and 20% of Super C45 conductive carbon, with an average loading of 5 mg cm^{-2}.

1 M $LiPF_6$ in ethylene carbonate (EC): dimethyl carbonate (DMC) 1:1 (LP30, UBE), and VC (Solvionic) were used as received. LiTFSI (> 99% battery grade, 3M), LiFSI and LiFTFSI (both from Provisco CS Ltd.) were pre-dried under rotary vane pump vacuum for 12 h and subsequently dried under the turbomolecular pump (< 10^{-7} mbar) for at least 20 h. All electrolytes formulations were prepared by adding 2 wt% of each additive into the pristine electrolyte in an argon-filled glove-box (O_2 and H_2O levels below 0.1 ppm), followed by mixing prior to use.

2.2. Electrochemical tests

Coin cells (type 2032) were assembled in an argon filled glove-box by sandwiching a glass fiber separator (Whatman GF/D) soaked with 100 µL of electrolyte between graphite or LFP electrodes (1.13 cm^2) and Li electrode (1.54 cm^2, Rockwood Lithium). Coin cells were used also for the assembly of the graphite/LFP Li-ion cells.

All cycling tests were conducted by storing the cells inside a climatic chamber (Binder) at 20 ± 1 °C. The cells were left at open circuit voltage (OCV) for 16 h (half-cells) or 24 h (Li-ion cells) prior to the measurements, which were conducted using a Maccor Series 4300 Battery Tester. The applied cycling protocol for half-cells is illustrated in Table S1 of the Supporting Information. The cycling rate of 1C corresponded to specific currents of 372 mA g^{-1} and 170 mA g^{-1} for graphite and LFP electrodes, respectively.

The Li-ion cells were initially charged/discharged at 20 ± 1 °C at C/20, then C/2, and, finally, at 1C rates (cathode-limited cells, i.e., 1C equals 170 mAh g^{-1}). After 10 cycles at 1C rate some cells were placed at 40 ± 1 °C and thermally equilibrated for 6 h. Then these cells were cycled at C/2 for 3 cycles, followed by long-term cycling at 1C.

The electrolytes' electrochemical stability window (ESW) was measured using three-electrode Swagelok cells with Pt (0.0078 cm^2) or carbon (1.13 cm^2) as working electrodes and Li metal as counter and reference electrode. The cells were characterized by linear sweep voltammetry using the VMP-3 potentiostat (BioLogic) from OCV to either −1.0 V or 6.0 V (using a fresh cell for each cathodic or anodic scan) with a scanning rate of 0.1 mV s^{-1}.

Electrochemical impedance spectroscopy (EIS) measurements were conducted using specially designed cells (ECC-PAT-Core, EL-CELL). The cell assembly procedure and scheme are described in detail in Fig. S2 of the Supporting Information. The cells were subjected to a rest period (12 h at 20 °C) prior to cycling of the graphite electrode at a rate of C/20 (using a Modulab, Solartron). The cycle was interrupted at different cell potentials (0.7, 0.5, and 0.01 V *vs* Li/Li^+ upon lithiation) and the cell was let to rest for 2 h at open circuit potential (OCP) prior to impedance measurements made using an AC amplitude of 5 mV in the frequency range of 10 kHz–0.1 Hz.

2.3. Differential scanning calorimetry (DSC) measurements

Electrodes from Li/graphite coin cells (type 2032) were used in this study. The graphite electrodes were subjected to a single lithiation at C/20 down to 0.01 V. The cells were then carefully disassembled in a glove-box. The lithiated graphite (Li_xC_6) powders, obtained by scratching the active material from the current collectors, were directly placed in closed, high-pressure DSC pans. The experiments were performed with a Discovery DSC (TA Instruments) and conducted by heating the sample at 5 K min^{-1} up to 300 °C under constant helium flow.

2.4. X-ray photoelectron spectroscopy (XPS) conditions

To analyze the SEI composition, Li/graphite half-cells were subjected to one lithiation-delithiation cycle as described in Table S1. To investigate the SEI evolution upon cycling, some cells were exposed to additional 50 cycles at C/2, also including the constant voltage step

upon lithiation. After cycling the cells were disassembled in the glovebox. The extracted graphite electrodes were carefully rinsed with 200 μL of DMC and dried in vacuum. The electrodes were then placed in an airtight vessel and transferred to the XPS sample chamber. The measurements were performed using a PHI 5800 MultiTechnique ESCA System with monochromatized Al-Kα (1486.6 eV) radiation. The detection angle of the measurement was 45° and pass energies of 93.9 and 29.35 eV were used for survey and detailed spectra, respectively. XPS spectra were also collected after sputtering the electrodes for 3 and 10 min. The binding energies were calibrated to the C1s signal of graphite at 284.6 eV and analyzed using CasaXPS software.

3. Results and discussion

3.1. Electrochemical performance

The effect of the additives on the electrochemical stability window (ESW) of the electrolytes was determined via linear sweep voltammetry (LSV), using a freshly assembled cell for each anodic and cathodic sweep. Several authors have pointed out that the working electrodes used for the measurements affect the results, e.g., platinum is more sensitive to degradation reaction than glassy carbon [22,23]. Therefore, we compared the results obtained using Pt (see Fig. S3 in Supporting Information) and carbon working electrodes. Using Pt, all electrolytes appear to be stable between 0.5 and 5.0 V *vs* Li/Li^+. Instead, when using carbon a narrower ESW (about 3 V) was obtained as shown in Fig. 1. Indeed, the electrolyte degradation occurs readily on the high surface area of the carbon electrode (at both high and low potentials), where the latter is also a better model than Pt for the conditions in a real Li-ion cell. Below 1.5 V *vs* Li/Li^+, as highlighted in the inset of Fig. 1, all electrolytes display reduction peaks related to the SEI formation on the carbon surface. The bare electrolyte shows the typical EC reduction peak at 0.65 V *vs* Li/Li^+, which is shifted to higher potential (~0.8 V *vs* Li/Li^+) when vinylene carbonate (VC) is added. The latter decomposes at about 1.0 V *vs* Li/Li^+, as indicated by the broad peak in Fig. 1 and already reported in literature [11]. On the other hand, addition of imide salts to the electrolyte does not prevent the reduction of ethylene carbonate (EC). Indeed, the voltammograms of the bare LP30 electrolyte and those with imides are very similar.

In the anodic scan on Pt, the electrolytes with LiFSI and LiFTFSI show an increased stability compared to that of LiTFSI and VC (Fig. S3). In case of the carbon working electrode all electrolytes display current flow above 4.5 V *vs* Li/Li^+ due to the degradation of solvents and $LiPF_6$. A strong, well defined peak is displayed only by the VC-containing electrolyte at about 4.8 V *vs* Li/Li^+, which is related to the decomposition of this additive and formation of polyvinyl carbonate species [10]. The electrolytes with imide additives display higher current densities between 4.5 and 5.3 V *vs* Li/Li^+ than the bare electrolyte. This effect may originate from the poorer anodic stability of the bis-imide anions with respect to the PF_6^- anion. However, further and more detailed investigations on the anodic behavior of the electrolytes with imide salts additives are necessary, if their combination with cathode materials working at potential higher than 4.0 V needs to be exploited.

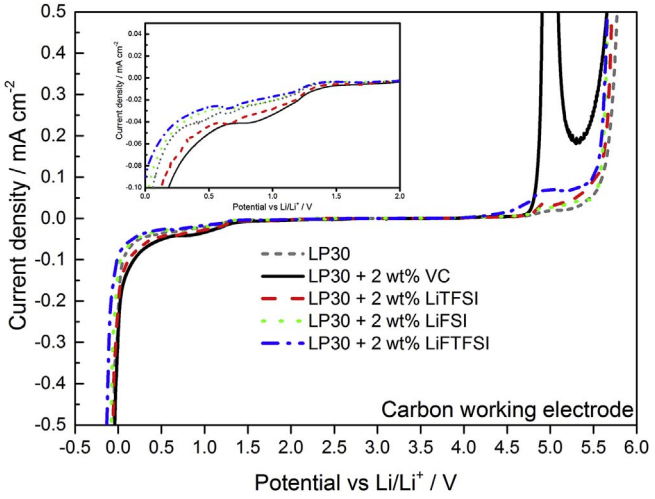

Fig. 1. Linear sweep voltammetry of the various electrolytes using carbon working electrodes.

Fig. 2 shows the electrochemical performance of graphite electrodes in the different electrolytes, comparing the 1st cycle voltage profiles. As mentioned in the introduction, the first cycle efficiency determines (mostly) how much lithium is consumed for the SEI build-up. This is a rather important characteristic, because the inefficiency must be balanced by extra cathode material in the Li-ion cell. For the additive-free electrolyte the efficiency is 93.3%; and the electrolyte doped with LiTFSI shows exactly the same value, while LiFSI and LiFTFSI offer slightly higher efficiencies (93.6% and 93.8%, respectively). On the other hand, the 1st cycle efficiency using VC is only 91.5%, indicating that a higher amount of Li^+ is depleted upon VC polymerization [24].

As reported in Fig. 2a, the cells with pure and imide-doped electrolytes show higher capacities than that with VC in the following cycles at C/2 and 1C rates. However, when the cycling rate further increases, a drop in capacity is observed for those employing LiFSI or LiFTFSI. The "fingerprint" cycles at C/2 show the same capacity for all cells, thus, degradation of graphite electrodes due to high cycling rates can be excluded. In the last part of the test (Fig. 2b), i.e., when the cells are cycled at C/2, the cell with VC shows a capacity decrease (partially recovered upon cycling), while a very stable cycling behavior is achieved with imide salts.

Fig. 2c shows that graphite displays a higher polarization below 0.2 V upon lithiation when VC is used, indicating a more resistive SEI than that obtained with other additives. This trend is maintained upon cycling (Fig. S4). The inset of Fig. 2c reports a portion of the differential capacity plots during the 1st cycle. In agreement with the ESW results in Fig. 1, a series of reduction peaks can be distinguished below 1.0 V. At around 0.9 V, the passivation of the graphite electrodes begins with decomposition of $LiPF_6$, as shown by the bare electrolyte trace [25]. For the electrolyte containing VC, this process is preceded by the VC decomposition, which results in the peaks overlapping [10,11]. Between 0.7 and 0.65 V the reduction of EC takes place. This is little affected in the presence of the Li-imide salts, but is almost suppressed for VC-containing electrolyte. Also for LiFSI- and LIFTFSI-containing electrolytes the intensity of this feature is lowered, suggesting that the decomposition of EC is, at least, reduced.

In order to study the impact of imide salts on the performance of full Li-ion cells, the behavior of $LiFePO_4$ (LFP) electrodes in these electrolytes was also tested. LFP electrodes display a better rate performance and stable cycling when the imide salts are added to the electrolyte as compared to VC (Fig. S5). The 1st cycle efficiencies are 99.0%, 98.6%, 97.3% and 96.8% for LiTFSI, VC, LiFSI and LiFTFSI, respectively.

To evaluate the influence of the additives on the long-term cycling performance, full cells comprising a graphite anode and a LFP cathode were assembled and tested. The cycling behavior at 20 and 40 °C is shown in Fig. 3.

As reported in Table 1, at 20 °C (Fig. 3a) the cell with the electrolyte doped with LiTFSI shows the highest 1st cycle efficiency and the most stable cycling performance in agreement with the half-cell results (the voltage profiles of the full-cells upon cycling are reported in Fig. S6). When LiFSI or LiFTFSI are used as additives, the long-term cycling stability is poorer than that obtained for the electrolyte with LiTFSI. At 40 °C, higher capacities are generally obtained. However, the temperature increase has a detrimental effect on the cycling stability, especially for the cells with imide salts, displaying at this temperature capacity retentions comparable to that of the cell with VC.

The electrochemical results presented so far confirm the beneficial

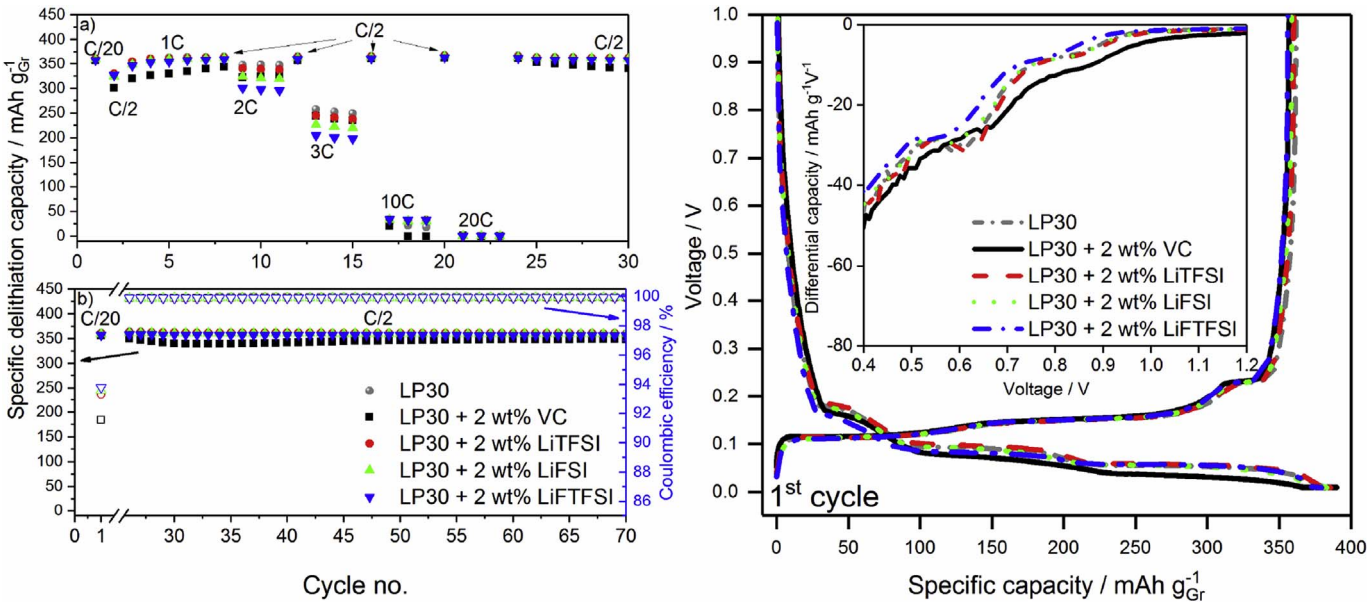

Fig. 2. Rate capability test (panel a), cycling performance (panel b) and voltage profiles (panel c) of graphite half-cells with different electrolyte additives. The inset in panel c shows a differential capacity plot.

effect of the use of imide salts, especially LiTFSI, as additives. Recently the reactivity of carbonate-based electrolytes containing lithium imides as main salts has been reported [26,27]. It has been shown that LiFSI and LiFTFSI are more prone to electrochemical reduction than LiTFSI at about 1 V *vs* Li/Li^+ due to the easier cleavage of the F-S bond than the F_3C-S bond. To understand if the origin of the improved half and full cell performance is related to the SEI layer characteristics, X-ray photoelectron spectroscopy (XPS) analysis was performed on the delithiated graphite electrodes extracted from the cells after the 1st or the 50th cycle.

3.2. Ex-situ surface analysis of cycled graphite electrodes

Fig. 4 compares the C1s spectra of the delithiated graphite electrodes extracted from the cell after the 1st or the 50th cycle. The

Table 1
Summary of the first cycle efficiency and capacity retention of the full cells with four electrolytes.

Electrolyte	1st cycle efficiency at 20 °C, %	Capacity retention (at the 600th *vs* the 20th cycle) at 20 °C, %	Capacity retention (at the 600th *vs* the 20th cycle) at 40 °C, %
LP30 + 2 wt% VC	86.3	79.6	78.7
LP30 + 2 wt% LiTFSI	88.7	98.1	79.7
LP30 + 2 wt% LiFSI	89.7	90.9	78.6
LP30 + 2 wt% LiFTFSI	88.0	86.3	79.9

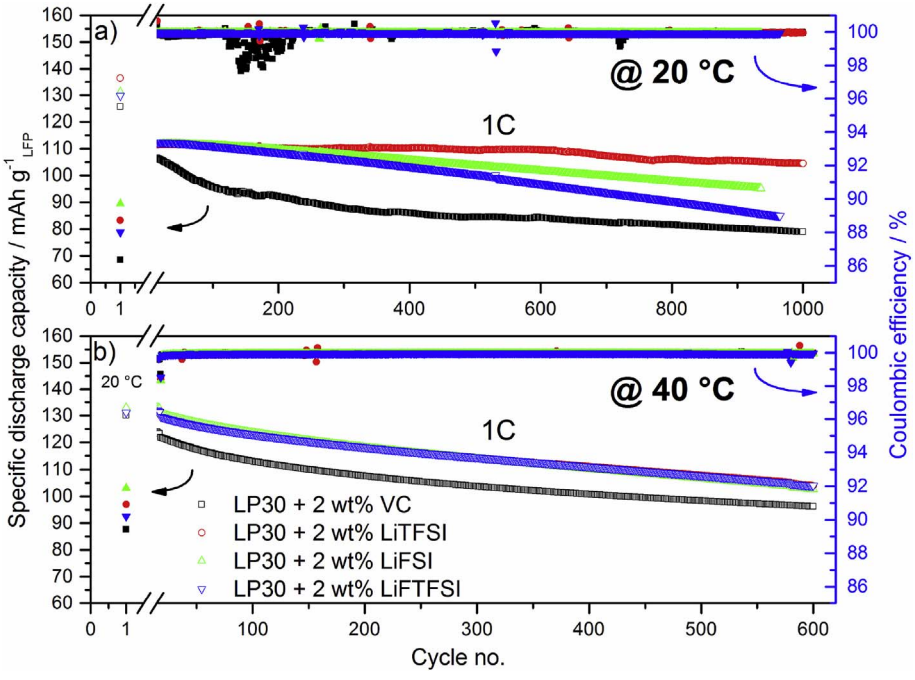

Fig. 3. Cycling performance of the full graphite/LFP cells at a) 20 °C and b) 40 °C.

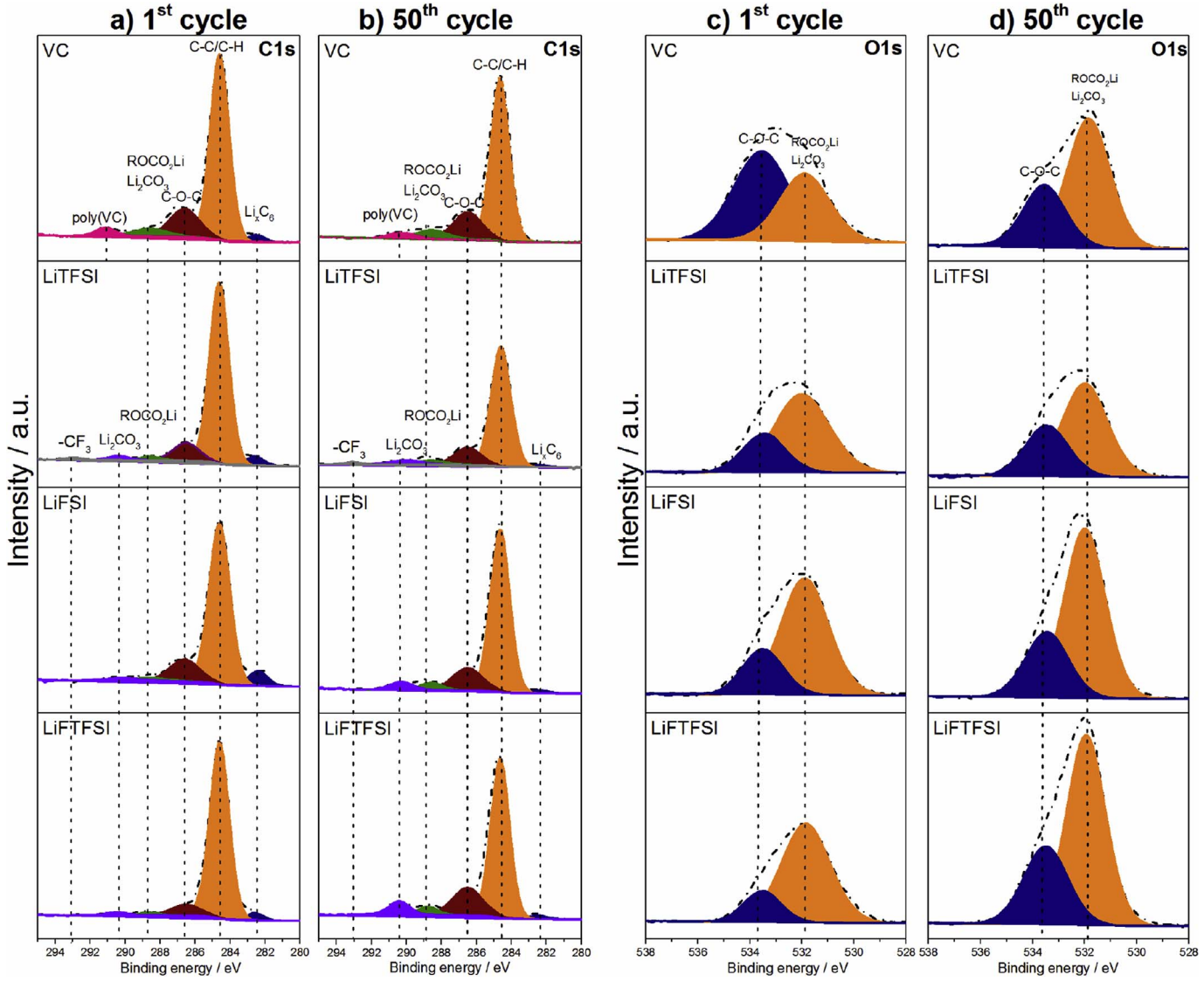

Fig. 4. C1s (a and b) and O1s (c and d) XPS spectra recorded on the graphite electrodes after the 1st or the 50th cycle with different electrolyte mixtures (cf. description in the figures).

dominant peak at 284.6 eV originates mainly from the sp^2 hybridized graphite, but also includes contributions from the CMC and conductive carbon added into the electrode composites. The peak at 282.5 eV is attributed to lithiated graphite species (i.e., Li_xC_6), suggesting that the delithiation was not fully completed. As these species refer to the graphite substrate and are not the SEI components, their appearance in the spectra suggests that the SEI is not very thick, especially on the electrode taken from the cell with LiFSI as additive. The broad feature at 286.6 eV is assigned mainly to the C atoms of the C-O-C groups in the poly(ethylene oxide), PEO, which is formed upon solvent polymerization [28–31]. The formation of PEO is also confirmed by the peak at 533.6 eV in the O1s XPS spectra in Fig. 4c. The rather broad peaks at 288.6 eV and 290.3 eV in Fig. 4a are assigned to carbon in C=O groups in organic lithium alkyl carbonates ($ROCO_2Li$) and lithium carbonates (Li_2CO_3) [29], respectively. The corresponding peak of the oxygen atoms in these groups is detected in the O1s spectra (Fig. 4c) at 531.8 eV. In the presence of imide salts in the electrolyte, the latter is the dominant peak in the O1s spectra, in contrast to the case of the electrolyte containing VC. In this electrolyte the formation of polymeric species resulting from the additive decomposition is indicated by the weak peak at 291.1 eV. In the O1s spectra this species should give a signal at 534.5 eV [11], which overlaps, however, with the C-O-C peak.

The main difference arising from the use of the three Li-imide salts is the peak at 293.2 eV detected only for the case of LiTFSI additive. In literature this peak is attributed to the $–CF_3$ group in the pristine salt, indicating that $TFSI^-$ is present on the electrode surface [29,32]. With this additive after 50 cycles (Fig. 4b) the C1s spectrum remains almost unchanged and the characteristic peak of pristine TFSI anion at 293.2 eV is retained. On the other hand, with all other electrolytes, the graphite surface becomes richer in carbonate species as confirmed by the increasing intensities of the corresponding peaks in the C1s and O1s spectra (Fig. 4b and d), indicating a pronounced SEI formation upon cycling. It is also interesting to note that the intensity of the lithiated graphite species in Fig. 4b decreases in all cases, due to a growth of the SEI layer with increasing charge/discharge cycle number.

The F1s spectra of graphite electrodes cycled in the various electrolytes are reported in Fig. 5a and b. The peak at 686.8 eV is assigned to residual $LiPF_6$ from incomplete salt removal during the electrode rinsing and/or intermediate decomposition products (Li_xPF_y), whose binding energies are close to that of $LiPF_6$ [29]. The peak at 684.9 eV is attributed to LiF, the main decomposition product of $LiPF_6$ [26].

In the presence of Li-imide salts additional peaks are seen at 688.6 eV for LiTFSI and LiFTFSI and at 687.8 eV for LiFSI. These peaks are attributed to the pristine salts or their incomplete decomposition products [26,27]. In the case of LiTFSI this peak is more pronounced, which is also supported by the detection of the $–CF_3$ peak in the C1s

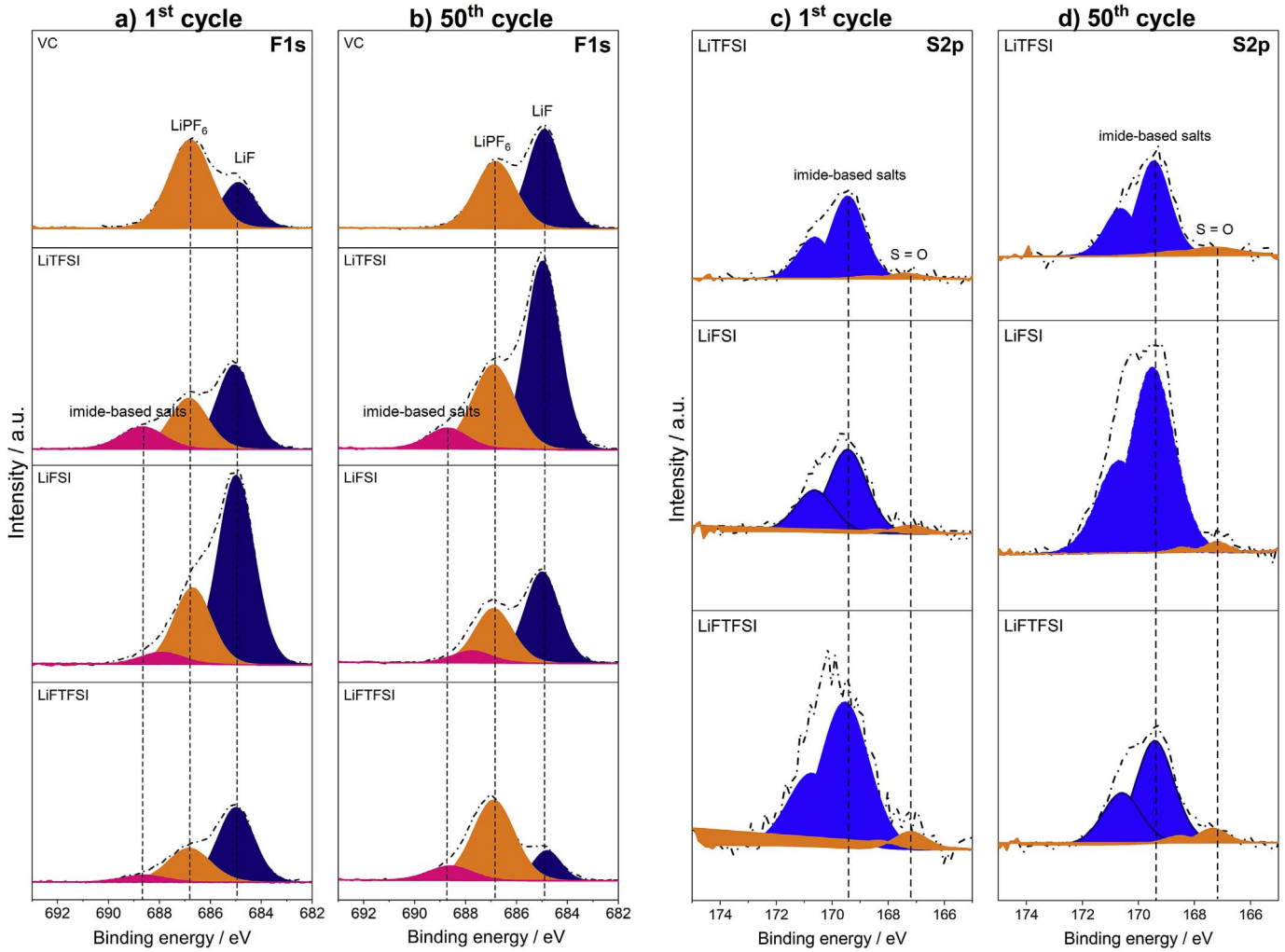

Fig. 5. F1s (a and b) and S2p (c and d) XPS spectra of graphite electrodes after the 1st or the 50th cycle with different electrolyte mixtures (cf. description in the figures).

spectra. This indicates that this salt does not decompose completely. The electrochemical reduction of LiFSI via S-F bond cleavage with LiF formation has been already reported by Philippe et al. [27]. This can, therefore, explain the high amount of LiF in the SEI when LiFSI is introduced in the electrolyte. Surprisingly, upon cycling the electrode surface is enriched in LiF in the presence of LiTFSI, but not with LiFSI and LiFTFSI (Fig. 5b). The P2p spectra (Figs. S7a and b) confirm the formation of the Li_xPF_y and $Li_xPF_yO_z$ in the SEI. The increase in the peak intensities of these components in P2p spectra, especially for LiFSI after the 1st cycle and LiTFSI after the 50th cycle is related to the increase of the LiF signal in the F2p spectra, indicating a more pronounced degradation of the main salt.

The S2p XPS spectra after one lithiation-delithiation cycle are reported in Fig. 5c. The $S2p_{3/2}$ peak at 169.3 eV is attributed to pristine imide salts [26] (in agreement with the F1s spectra), whereas the peak at 167 eV can be assigned to S = O bonds in decomposition products of Li-imide salts [17,26]. However, it has been reported that this peak may also arise from salt decomposition induced by the X-ray beam [27]. No significant change in the signal intensity is observed upon cycling (Fig. 5d).

The values of atomic concentrations, representing the composition of the SEI, are reported in Figs. S7 and S8 in the Supporting Information, including their evolution upon sputtering. It should be noted that the signal at 282.5 eV in the C1s spectra is attributed to the lithiated graphite species (Li_xC_6) and, thus, is mostly related to the electrode active material (graphite) rather than to the SEI, as mentioned above. Therefore, the value of this signal was subtracted from the overall atomic concentration of carbon (Fig. S8). Additionally, a corresponding fraction of the Li concentration (calculated assuming a LiC_6 stoichiometry) was also removed.

The atomic content (%) of the SEI components (Fig. S9) is useful to give an overall picture of the surface composition. The atomic concentrations of the SEI components obtained after the 1st cycle in the additive-free electrolyte (LP30) have also been included for a better comparison. The amount of carbonate species (both organic and inorganic ones) and PEO on the SEI after the 1st cycle decreases in the order VC > LiFSI > LiTFSI > LiFTFSI, while in bare electrolyte the SEI is predominated by organic and inorganic carbonates with a lower PEO fraction, in line with other reports [33,34]. In agreement with the previous discussion, LiF decreases in the order LiFSI > LiFTFSI > LiTFSI > VC > LP30. This also indicates that the initial SEI formed in the presence of imide salts is richer in LiF than that formed in the VC-containing or additive-free electrolyte.

The SEI formation is not completed after one cycle but continues upon further cycling. After 50 cycles, the electrodes exposed to Li-imide salts have a higher amount of carbonates on their surface than that with VC. Furthermore, with respect to the 1st cycle, a decrease of LiF by 12 at % and 43 at% is found for LiFSI and LiFTFSI, respectively, while 9 at% more LiF is present when using LiTFSI. Still, except for the LiFTFSI-containing electrolyte, the main component of the SEI layer is LiF also after 50 cycles.

The variation of the atomic concentrations upon sputtering gives

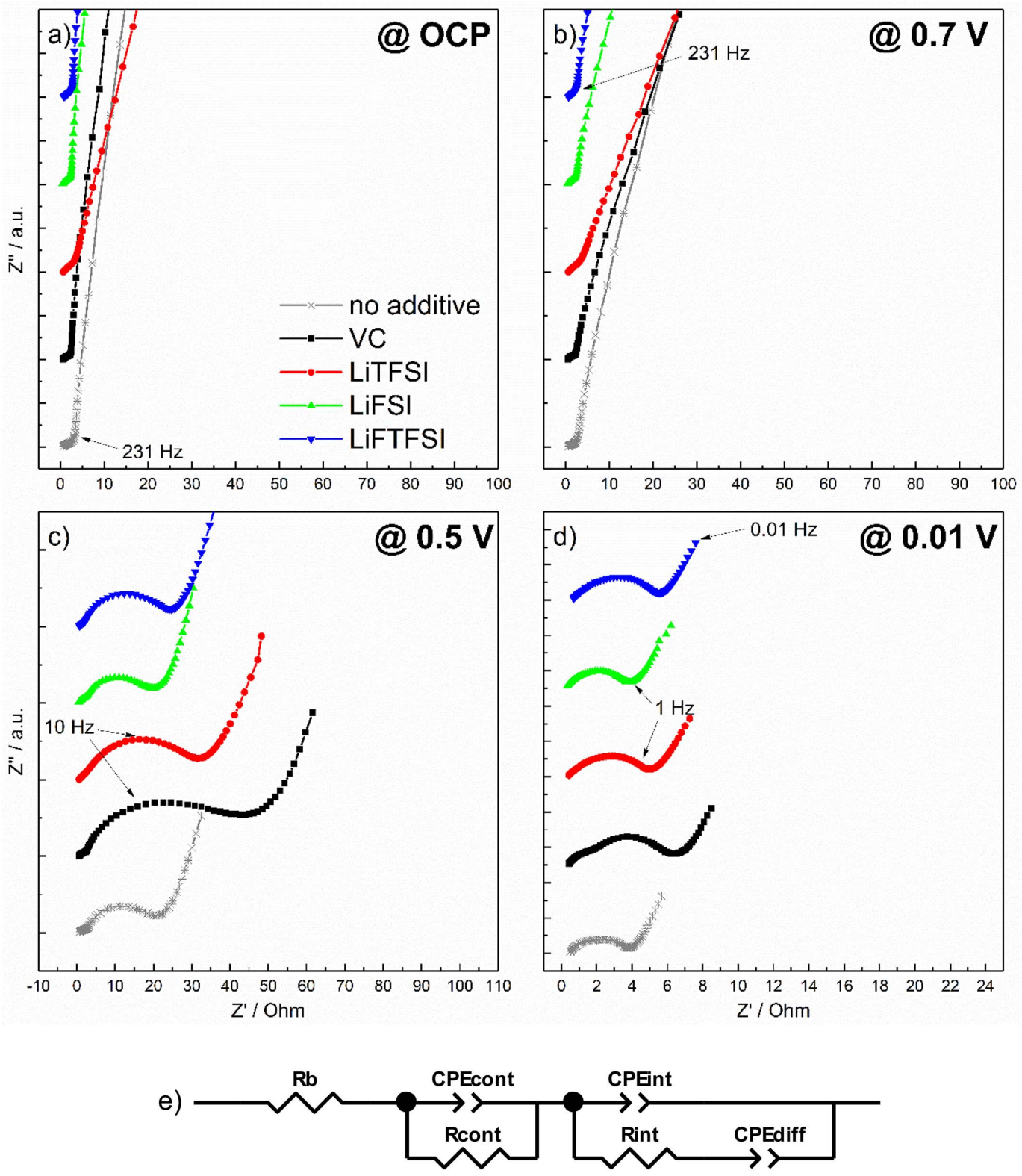

Fig. 6. Nyquist plots of graphite electrodes at a) OCP, b) 0.7 *vs* Li/Li^+, c) 0.5 *vs* Li/Li^+, d) 0.01 V *vs* Li/Li^+ and e) equivalent circuit model used for the fitting at 0.5 and 0.01 V *vs* Li/Li^+. The measurements were performed on three-electrode EL-cells with Li metal as RE and CE. Electrode area: 2.54 cm^2.

additional information about changes in the SEI composition with increasing depth. For the electrodes subjected to the 1st cycle, after 3 min of sputtering Li_xC_6 beneath the SEI layer gives a more intense signal for the electrodes exposed to imide salts-containing and additive-free electrolytes than for that of VC (Fig. S9a). This suggests that the passivation layer with VC additive is initially thicker. Upon cycling, e.g., after 50 cycles, the SEI keeps growing further. After 3 min of sputtering all electrodes show almost the same atomic concentration of Li_xC_6 (Fig. S9b). This indicates that the SEI in the presence of imide salts has grown more and become thicker than that with VC. The carbonates and PEO contents decrease upon prolonged cycling, showing that they are present in the most outer part of the passivation layer. Although it seems

Table 2
The interfacial resistances determined by EIS at 0.5 and 0.01 V *vs* Li/Li^+ with various electrolytes.

Electrolyte	R_{int} at 0.5 V *vs* Li/Li^+, Ohm	R_{int} at 0.01 V *vs* Li/Li^+, Ohm
LP30	19	2.8
LP30 + 2 wt% VC	39	4.6
LP30 + 2 wt% LiTFSI	30	4.6
LP30 + 2 wt% LiFSI	18	3.7
LP30 + 2 wt% LiFTFSI	22	4.8

Table 3
Heat generated upon heating lithiated graphite powders in the electrolytes.

Electrolyte	1st peak, J/g	2nd + 3rd peaks, J/g	Total, J/g
LP30	16	468	484
LP30 + 2 wt% VC	56	366	422
LP30 + 2 wt% LiTFSI	45	499	544
LP30 + 2 wt% LiFSI	49	506	555
LP30 + 2 wt% LiFTFSI	38	541	579

that the inner part of the SEI is rich in LiF, as its content increases after 3 min of sputtering, it should be kept in mind that LiF can be also formed upon Ar^+ etching [35].

To summarize, the XPS results reveal that the SEI obtained on the graphite surface after one cycle is thinner and richer in LiF when imide salts are used as additives. In all cases the passivation layer grows upon cycling, however, containing more organic and inorganic lithium carbonates in the topmost layers when the imide salts are added to the electrolyte.

It is known that insoluble LiF and Li_2CO_3 are rather stable SEI components, however, providing insufficient Li ion conduction. Recently, the synergetic effect of LiF and Li_2CO_3 in the SEI of Si anodes has been reported by Zhang et al. [36]. The authors reported that the combination of LiF and Li_2CO_3 promotes Li ion diffusion due to charge accumulation at the grain boundaries, and further stabilizes the SEI itself. Interestingly, according to Ref. [36] the higher was the LiF content (up to 15%), the lower was the 1st cycle irreversible capacity and the better the rate capability and the long-term capacity retention of the Si anode, which is in line with our results.

3.3. EIS characterization of graphite electrodes

The SEI composition and thickness obviously affect the impedance of the graphite electrodes. The EIS spectra, recorded at specific potentials, are shown in Fig. 6. The graphite electrodes were subjected to slow (C/20) lithiation. The impedance measured at open circuit potential (OCP), 0.7 V *vs* Li/Li^+ (after reduction of the additive/salt), 0.5 V *vs* Li/Li^+ (after solvent reduction) and in the fully lithiated state are illustrated in Fig. 6a–d.

At the OCP (Fig. 6a) only one open semicircle is observed in the high-to-middle frequency range. As previously proposed in literature, this depressed semicircle arises from the resistances which can be linked, for example, to particle-particle and particle-current collector contacts [37,38]. The depressed shape of the semicircle might, furthermore, arise from electrode porosity and inhomogeneous surface roughness. In the lower frequency range, where likely no faradaic reactions occur at this potential (ca. 3 V *vs* Li/Li^+), the graphite electrode approaches the blocking-electrode behavior [39,40].

At 0.7 V *vs* Li/Li^+ (Fig. 6b), the reductive decomposition reactions are initiated by electrolyte solvents and $LiPF_6$, as indicated by the broad peak in the differential capacity plot in the inset of Fig. 2c. Furthermore, VC decomposition takes place at this potential [11]. Here, the impedance response of graphite electrodes cycled with different electrolytes does not substantially differ from those recorded at the OCP indicating that, if formed, the SEI is very porous and permeable to the electrolyte.

At 0.5 V *vs* Li/Li^+ (Fig. 6c), besides the high frequency semicircle associated with contact resistance, a new element in the middle-frequency range appears for all electrodes. At this potential, according to the differential capacity plot, the electrolyte reduction should be mostly completed, but the typical staging intercalation into graphite has not started yet. Therefore, it is reasonable to attribute this new semicircle to the freshly formed SEI and Li^+ (charge) transfer at the interface. The separation of these contributions is, unfortunately, hindered by the considerable overlapping of the two semicircles probably due to their very similar time constants.

In the fully lithiated state (at 0.01 V *vs* Li/Li^+), the same semicircles

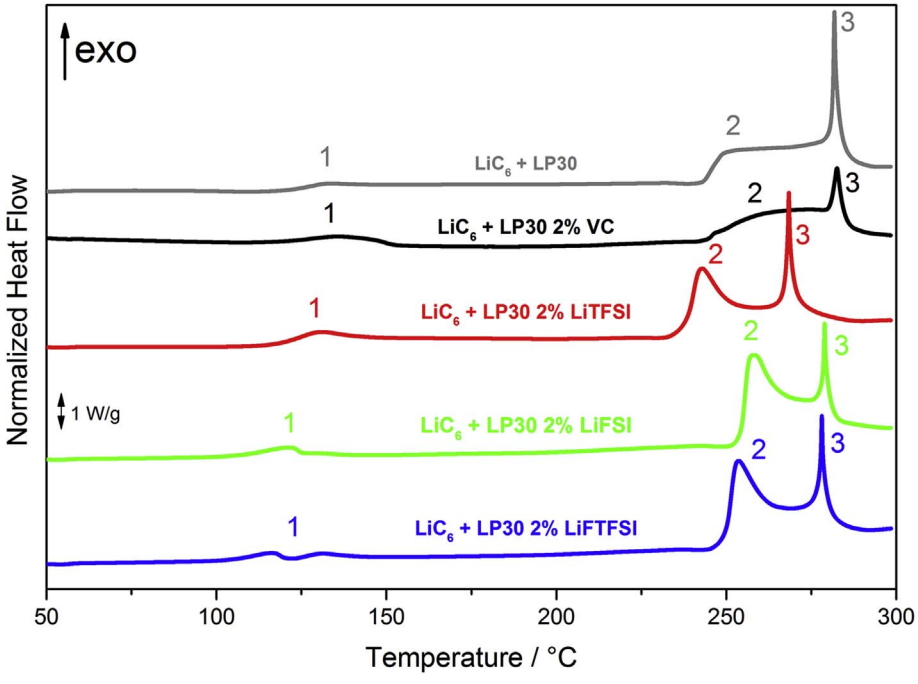

Fig. 7. DSC traces of lithiated graphite powders in contact with the different electrolytes indicated in the figure.

can be observed in Fig. 6d. The semicircles related to the interfacial resistance are smaller for all electrolytes as compared to the responses at 0.5 V *vs* Li/Li^+. This might be related to the reconstruction of the SEI upon further graphite electrode polarization with formation of the inorganic species, which have high ionic and low electronic conductivity [4,39]. Additionally, charge transfer through the completed SEI is faster, also contributing to the shrinkage of the spectra in the fully lithiated state [41].

Fig. 6e shows the equivalent circuit model used for fitting the spectra at 0.5 and 0.01 V *vs* Li/Li^+. It consists of a resistor (intercept with the real axis Z′) describing the bulk resistance of the cell (R_b), mostly accounting for the electrolyte contribution [39,40] and two R|Q elements connected in series. The first R|Q element is constituted by a resistor (R_{cont}) in parallel with a constant phase element (CPE_{cont}), accounting for the various contact issues described above. The second R|Q element, also consisting of a resistor (R_{int}) and a constant phase element (CPE_{int}) in parallel, is attributed to the interfacial processes previously mentioned (SEI and charge transfer). To compensate for the non-ideal behavior, the straight line at low frequencies attributed to the lithium ion diffusion into graphite is also modeled with a constant phase element (CPE_{diff}) rather than with a Warburg element.

As shown in Table 2, at 0.5 V *vs* Li/Li^+ the VC-containing electrolyte shows the highest R_{int}, which is related to the formation of the polymeric surface film upon the additive decomposition, confirming the prediction of a more resistive SEI from the voltage profile in Fig. 2c. Interestingly, the interfacial resistance of the bare electrolyte at this potential is comparable to that of the LiFSI-containing one, thus indicating the formation of a more ionically conductive SEI. In the fully lithiated state a sharp decrease in the impedance is observed, which is mostly related to the higher electronic conductivity of the Li-intercalated graphite [42], and reconstruction of the SEI. The smallest interfacial resistance of the bare electrolyte at 0.01 V *vs* Li/Li^+ might be related to the high amount of carbonates on the surface, as determined by XPS, which are known to possess relatively high ionic conductivity [36]. In case of imide salts the interfacial resistances are comparable to that obtained in presence of VC with slightly lower value for LiFSI-containing electrolyte.

3.4. Thermal behavior of lithiated graphite in contact with the electrolytes

The thermal stability of the SEI is of great importance for the battery safety. The thermal decomposition of the SEI may lead to uncontrolled exothermic reactions between the anode and the electrolyte, possibly resulting in a thermal runaway of the cell. Fig. 7 shows the DSC profiles of the graphite electrodes electrochemically lithiated in the presence of the various electrolytes. For the bare electrolyte we observe a weak exothermic peak at around 140 °C with a slight change of the baseline (marked as “1”). This peak has been attributed to the rupture of the SEI layer, leading to further reactions between the electrolyte and the lithiated graphite [43–45]. Using VC as additive, this peak becomes broader. In the case of LiTFSI, the onset of SEI cracking is almost unchanged, while for LiFSI and LiFTFSI it occurs at slightly lower temperatures. Furthermore, in the case of LiFTFSI, two distinct thermal events can be distinguished at this temperature. Above 230 °C, a broad exothermic peak (marked as “2”), followed by a sharp intense peak (marked as “3”) are observed, which are related to the thermal decomposition of the electrolyte and SEI breakdown [44]. Using VC, the intensity of peak “3” is lower, which is in line with the results of other studies reporting that VC-derived SEIs are more thermally stable than those formed in the VC-free electrolytes [10,11]. When LiTFSI is used, the onset of these reactions is shifted to lower temperatures. Furthermore, the intensity of peak “2” increases for the electrolytes containing imide salts compared to pure LP30 and VC-containing ones. Overall, this behavior indicates that the thermal stability of the lithiated graphite anode is slightly reduced by the addition of Li-imide salts in the electrolyte with respect to the pristine or VC-doped electrolytes. The total heats reported in Table 3 show that more energy is released above 230 °C using the imide salts as compared to VC. However, additional investigations are necessary to explore in-depth the synergetic effect of including simultaneously VC and Li-imide salts in the electrolyte formulation to balance the beneficial properties of these additives.

4. Conclusions

The results of this work prove that the use of Li-imide salts as electrolyte additives is beneficial for the long-term cycling stability of graphite/$LiFePO_4$ cells. At 20 °C, LiTFSI leads to the capacity fading of only 2% after 600 cycles, while the control cell with VC loses 20% of the initial capacity. Moreover, the 1st cycle coulombic efficiency is improved with respect to that obtained using VC additive. However, the positive effect of the imide salts on the capacity retention is hidden at 40 °C due to the higher ionic conductivity of the electrolytes and overall improved kinetics of the reactions at the electrodes. The presence of imide-based Li salts in the electrolyte does not shrink the electrochemical stability window but the resulting SEI is slightly less thermally stable than that obtained using VC. XPS analysis reveals that with Li-imide salts thin, LiF- and carbonates-rich SEI layers on the graphite electrodes are obtained. In addition, impedance spectroscopy evidences that the SEI obtained in the presence of the Li-imide salts is less resistive than the one originating from the electrolyte with VC additive.

It can be inferred that the origin of the improved performance of the cells containing imide salts is linked to the presence of higher amount of LiF, which seems to promote the Li^+ diffusion across the SEI.

Acknowledgements

The authors acknowledge the financial support from the EU under the grant agreement no. 653373 (SPICY – Silicon and polyanionic chemistries and architectures of Li-ion cell for high energy battery). CEA-LITEN (17 rue des Martyrs F-38054 Grenoble France) is acknowledged for kindly providing the graphite and $LiFePO_4$ electrodes. Imerys and Rockwood Lithium are also acknowledged for kindly supplying Super C45 and the lithium foil, respectively.

Appendix A. Supplementary data

Supplementary data related to this article can be found at http://dx.doi.org/10.1016/j.jpowsour.2017.11.045.

References

[1] J.M. Tarascon, M. Armand, Nature 414 (2001) 359–367.
[2] N. Nitta, F. Wu, J.T. Lee, G. Yushin, Mater. Today 18 (2015) 252–264.
[3] M. Armand, J. Chabagno, N. Duclot, M. Vashishta (Ed.), Fast Ion Transport in Solids, Shenoy, North-Holland, Amsterdam, 1979, p. 131.
[4] S.J. An, J. Li, C. Daniel, D. Mohanty, S. Nagpure, D.L. Wood Iii, Carbon 105 (2016) 52–76.
[5] P. Verma, P. Maire, P. Novák, Electrochim. Acta 55 (2010) 6332–6341.
[6] J. Kalhoff, G.G. Eshetu, D. Bresser, S. Passerini, ChemSusChem 8 (2015) 2154–2175.
[7] R. Younesi, G.M. Veith, P. Johansson, K. Edstrom, T. Vegge, Energy & Environ. Sci. 8 (2015) 1905–1922.
[8] Y. Ein-Eli, Electrochem. Solid-State Lett. 2 (1999) 212–214.
[9] S. Bhattacharya, A.T. Alpas, Carbon 50 (2012) 5359–5371.
[10] D. Aurbach, K. Gamolsky, B. Markovsky, Y. Gofer, M. Schmidt, U. Heider, Electrochim. Acta 47 (2002) 1423–1439.
[11] H. Ota, Y. Sakata, A. Inoue, S. Yamaguchi, J. Electrochem. Soc. 151 (2004) A1659–A1669.
[12] A.M. Haregewoin, A.S. Wotango, B.-J. Hwang, Energy & Environ. Sci. 9 (2016) 1955–1988.
[13] H.-B. Han, S.-S. Zhou, D.-J. Zhang, S.-W. Feng, L.-F. Li, K. Liu, W.-F. Feng, J. Nie, H. Li, X.-J. Huang, M. Armand, Z.-B. Zhou, J. Power Sources 196 (2011) 3623–3632.
[14] M. Dahbi, D. Violleau, F. Ghamouss, J. Jacquemin, F. Tran-Van, D. Lemordant, M. Anouti, Ind. Eng. Chem. Res. 51 (2012) 5240–5245.
[15] J.C. Burns, N.N. Sinha, G. Jain, H. Ye, C.M. VanElzen, W.M. Lamanna, A. Xiao, E. Scott, J. Choi, J.R. Dahn, J. Electrochem. Soc. 159 (2012) A1095–A1104.
[16] A. Moretti, S. Jeong, G.A. Giffin, S. Jeremias, S. Passerini, J. Power Sources 269

(2014) 645–650.
[17] M. Nie, B.L. Lucht, J. Electrochem. Soc. 161 (2014) A1001–A1006.
[18] J. Kalhoff, D. Bresser, M. Bolloli, F. Alloin, J.-Y. Sanchez, S. Passerini, ChemSusChem 7 (10) (2014) 2939–2946.
[19] M. Dahbi, F. Ghamouss, F. Tran-Van, D. Lemordant, M. Anouti, J. Power Sources 196 (2011) 9743–9750.
[20] J.C. Burns, G. Jain, A.J. Smith, K.W. Eberman, E. Scott, J.P. Gardner, J.R. Dahn, J. Electrochem. Soc. 158 (2011) A255–A261.
[21] D.Y. Wang, A. Xiao, L. Wells, J.R. Dahn, J. Electrochem. Soc. 162 (2015) A169–A175.
[22] N. De Vos, C. Maton, C.V. Stevens, ChemElectroChem 1 (2014) 1258–1270.
[23] M.P.S. Mousavi, A.J. Dittmer, B.E. Wilson, J. Hu, A. Stein, P. Bühlmann, J. Electrochem. Soc. 162 (2015) A2250–A2258.
[24] L. El Ouatani, R. Dedryvère, C. Siret, P. Biensan, S. Reynaud, P. Iratçabal, D. Gonbeau, J. Electrochem. Soc. 156 (2009) A103–A113.
[25] S.A. Delp, O. Borodin, M. Olguin, C.G. Eisner, J.L. Allen, T.R. Jow, Electrochim. Acta 209 (2016) 498–510.
[26] G.G. Eshetu, T. Diemant, S. Grugeon, R.J. Behm, S. Laruelle, M. Armand, S. Passerini, ACS Appl. Mater. Interfaces 8 (2016) 16087–16100.
[27] B. Philippe, R. Dedryvère, M. Gorgoi, H. Rensmo, D. Gonbeau, K. Edström, J. Am. Chem. Soc. 135 (2013) 9829–9842.
[28] R. Dedryvère, S. Leroy, H. Martinez, F. Blanchard, D. Lemordant, D. Gonbeau, J. Phys. Chem. B 110 (2006) 12986–12992.
[29] D. Ensling, M. Stjerndahl, A. Nyten, T. Gustafsson, J.O. Thomas, J. Mater. Chem. 19 (2009) 82–88.
[30] C.M. Ghimbeu, C. Decaux, P. Brender, M. Dahbi, D. Lemordant, E. Raymundo-Piñero, M. Anouti, F. Béguin, C. Vix-Guterl, J. Electrochem. Soc. 160 (2013) A1907–A1915.
[31] H. Kim, S. Grugeon, G. Gachot, M. Armand, L. Sannier, S. Laruelle, Electrochim. Acta 136 (2014) 157–165.
[32] Y. Pan, G. Wang, B.L. Lucht, Electrochim. Acta 217 (2016) 269–273.
[33] E. Markevich, K. Fridman, R. Sharabi, R. Elazari, G. Salitra, H.E. Gottlieb, G. Gershinsky, A. Garsuch, G. Semrau, M.A. Schmidt, D. Aurbach, J. Electrochem. Soc. 160 (2013) A1824–A1833.
[34] M. Nie, D.P. Abraham, Y. Chen, A. Bose, B.L. Lucht, J. Phys. Chem. C 117 (2013) 13403–13412.
[35] K. Edström, M. Herstedt, D.P. Abraham, J. Power Sources 153 (2006) 380–384.
[36] Q. Zhang, J. Pan, P. Lu, Z. Liu, M.W. Verbrugge, B.W. Sheldon, Y.-T. Cheng, Y. Qi, X. Xiao, Nano Lett. 16 (2016) 2011–2016.
[37] M. Gaberscek, J. Moskon, B. Erjavec, R. Dominko, J. Jamnik, Electrochem. Solid-State Lett. 11 (2008) A170–A174.
[38] S. Dsoke, X. Tian, C. Täubert, S. Schlüter, M. Wohlfahrt-Mehrens, J. Power Sources 238 (2013) 422–429.
[39] S.S. Zhang, K. Xu, T.R. Jow, Electrochim. Acta 51 (2006) 1636–1640.
[40] S.S. Zhang, J. Power Sources 163 (2007) 713–718.
[41] M. Umeda, K. Dokko, Y. Fujita, M. Mohamedi, I. Uchida, J.R. Selman, Electrochim. Acta 47 (2001) 885–890.
[42] S. Basu, C. Zeller, P.J. Flanders, C.D. Fuerst, W.D. Johnson, J.E. Fischer, Mater. Sci. Eng. 38 (1979) 275–283.
[43] Z. Zhang, D. Fouchard, J.R. Rea, J. Power Sources 70 (1998) 16–20.
[44] J.-i. Yamaki, H. Takatsuji, T. Kawamura, M. Egashira, Solid State Ionics 148 (2002) 241–245.
[45] U. von Sacken, E. Nodwell, A. Sundher, J.R. Dahn, J. Power Sources 54 (1995) 240–245.